Electronic Supplementary Information for

How big is the substituent dependence of the solar photolysis rate of Criegee intermediates?

Cangtao Yin[1] and Kaito Takahashi[1]*

[1] Institute of Atomic and Molecular Sciences, Academia Sinica, Taipei 10617, Taiwan

*To whom correspondence should be addressed: kt@gate.sinica.edu.tw

Abstract: In the supplementary material we present the details of the quantum chemistry calculations, as well UV spectra calculation methods. Also, several tests concerning the convergence will be provided to justify the credibility of the results given in the main text.

Table of Contents

Theoretical Methods

In Figure S1, we present the schematic geometries of all the Criegee intermediates (CIs) studied in the present paper. For CH_3CHOO and CHCCHOO there are two conformations, *anti*- and *syn*- depending on the position of the hydrocarbon group with respect to the OO bond. For CH_3CH_2CHOO and $CH_2CHCHOO$ the terminal hydrocarbon group can give two more different conformations.

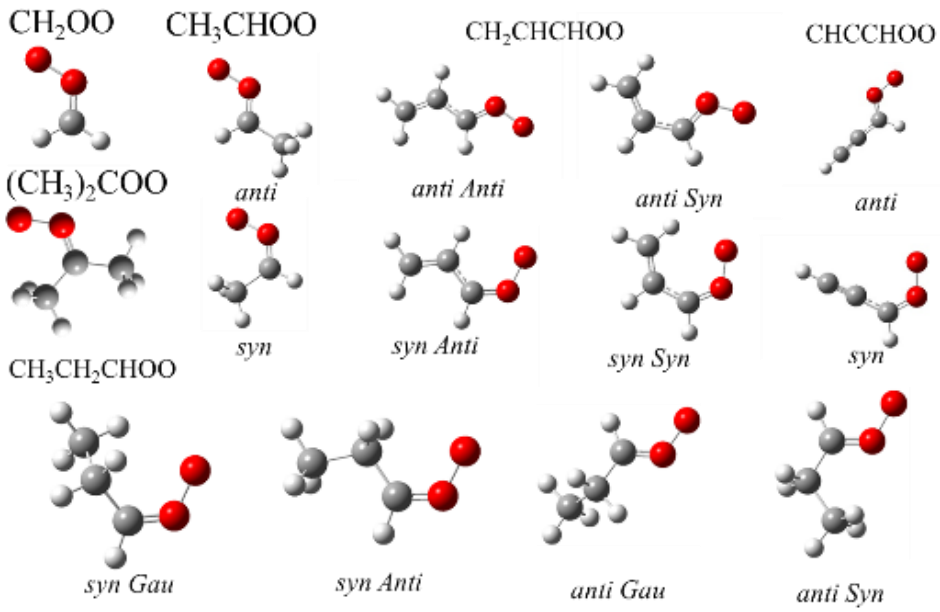

Figure S1. Schematic diagram of CH_2OO, $(CH_3)_2COO$, CH_3CHOO, $CH_2CHCHOO$, CHCCHOO, and CH_3CH_2CHOO.

As mentioned in the main text the calculation for the UV spectra depends on the quantum chemistry method that is used to calculate the potential energy surface (PES) and the transition moment (TM) function, as well as the quantum wavepacket dynamics used to calculate the UV spectra.

Quantum chemistry methods:

We will report the studies done to test the convergene of our results. First for CH_2OO, we performed five CASSCF calculations: 1) full valance by closing 1s orbitals of C and O atoms (18e 14o); 2) closing 1s and 2s orbitals of C and O atoms (12e 11o); 3) closing 1s, 2s and 1of 2p orbitals of C and O atoms (10e 10o); 4) closing 1s, 2s and 2 of 2p orbitals of C and O atoms, and excluding one virtual orbital (8e 8o); 5) closing 1s, 2s and 3of 2p orbitals of C and O atoms, and excluding two virtual orbitals (6e 6o). We found that except for the last one, the difference due to the active spaces

is very small, which gives us confidence in using smaller active space when calculating other CIs. Therefore, for CH_3CHOO, we chose the third active space (14e 15o), which gave spectra which are in agreement with the experimental data, see figure 4 (b) and (f) of the main text. For CHCCHOO, we also tried to use the third active space; however since it has more virtual orbitals than CH_3CHOO, we had to exclude several virtual orbitals at high energy due to computational limitations. We tested that excluding two (14e 14o) and three (14e 13o) virtual orbitals only result in minor variations in the spectra. For $CH_2CHCHOO$, we chose the fourth active space and also confirmed that excluding two (14e 15o) and three (14e 14o) virtual orbitals only give minor variations. However, for CH_3CH_2CHOO and $(CH_3)_2COO$, we can only perform the fifth active space due to the limitation of our computational resource. Therefore, the theoretical UV spectrum of $(CH_3)_2COO$ is blue shifted by about 25 nm compared to the experimental one, see figure 4 (e) of the main text. We confirmed again that excluding two (14e 16o) or three (14e 15o) virtual orbitals do not change the general feature.

The active space in MRCI calculation, however, has a different story. It seems that the calculated spectra is insensitive to the MRCI active space. It turns out that other than CHCCHOO, the difference caused by (8e, 8o) and (10e, 10o) active space is very small, see figure S2.

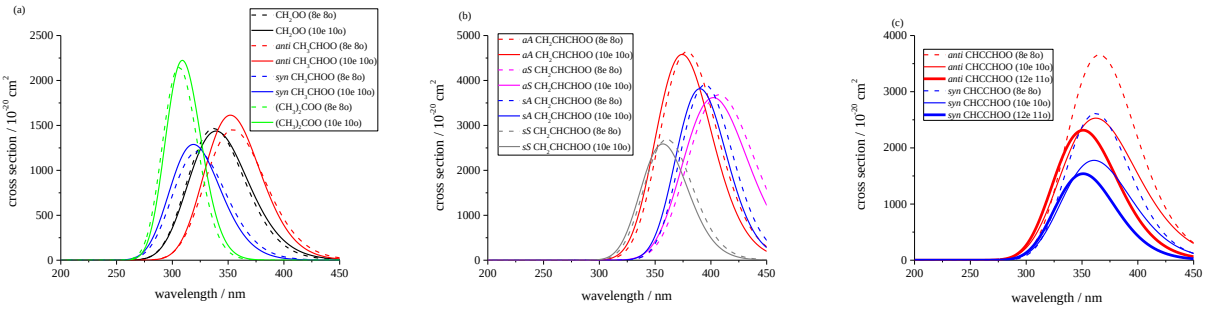

Figure S2. UV spectra calculated using the Gaussian function using equilibrium geometry values for the excitation energy and transition moment for (a) CH_2OO, CH_3CHOO and $(CH3)_2COO$ (b) $CH_2CHCHOO$ and (c) CHCCHOO. Results for (8e 8o) active space are given with dashed lines, those with the (10e 10o) active space are given in solid lines, and two (12e 11o) active space results are given in thicker solid lines for CHCCHOO.

UV spectra calculation methods:

We present the details concerning the convergence of UV spectra calculation methods. Below is the results of a wave packet simulation.

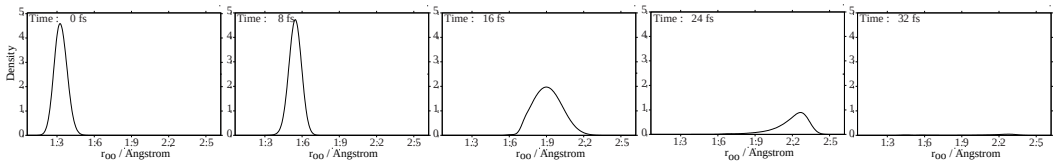

Figure S3. Schematic diagram of the wave packet propagation for CH_2OO.

In Figure S4, we present the results obtained by the FA and WPA calculation. One can notice that spectral features originate from the transition from the GS zero-point vibrational state to the different vibrational excited states on 2A'. For the high energy states, at 300 to 350 nm, the lifetime is short, thereby resulting in a broad peak. On the other hand, for the low energy peaks, 350 to 400 nm, the lifetime is longer, which results in sharper peaks. As a consequence, in the wave packet dynamics, one sees oscillations in the red region of the peak.

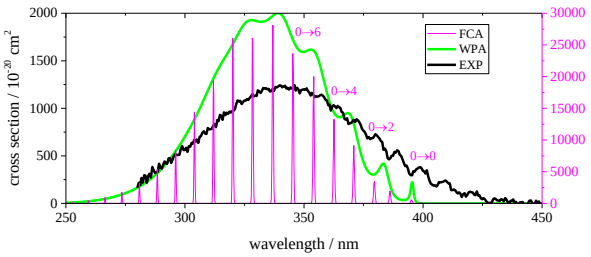

Figure S4. The spectra obtained for the wave packet and Franck-Condon approximations for CH_2OO. The experimental spectra of Ting et al.[1] are also given in black lines.

To verify that the inclusion of the COO bending angle, θ_{COO}, will not greatly affect the obtained UV spectra, we also performed a calculation using an effective 2D Hamiltonian for the CH_2OO molecule. The kinetic energy term was obtained using a triatomic Hamiltonian given by Handy[2] and only considered the COO portion of CH_2OO.

$$\widehat{H} = -\frac{\hbar^2}{2m_{OO}}\frac{\partial^2}{\partial {r_{OO}}^2} - \frac{\hbar^2}{2}\left[\frac{1}{m_{OO}{r_{OO}}^2} + \frac{1}{m_{CO}{r_{CO}}^2}\right]\frac{\partial^2}{\partial {\theta_{COO}}^2} + \frac{\hbar^2\cos\theta_{COO}}{m_O r_{CO} r_{OO}}\frac{\partial^2}{\partial \theta_{COO}\partial r_{OO}}$$

$$+\frac{\hbar^2\cos\theta_{COO}}{m_O r_{CO}}\frac{\partial}{\partial r_{OO}} - \frac{\hbar^2}{2\tan\theta_{COO}}\left[\frac{1}{m_{OO}{r_{OO}}^2} + \frac{1}{m_{CO}{r_{CO}}^2}\right]\frac{\partial}{\partial \theta_{COO}}$$

$$-\frac{\hbar^2}{2}\left[\frac{4\sin\theta_{COO}}{m_O r_{OO} r_{CO}} - \frac{2}{m_O r_{OO} r_{CO}\sin\theta_{COO}}\right]\frac{\partial}{\partial \theta_{COO}}$$

$$+V(r_{OO},\theta_{COO})$$

Similarly for the CCO bending angle, θ_{CCO}, and r_{OO}, we used the following Hamiltonian which was derived for a tetraatomic molecule by Handy[2]

$$\widehat{H} = -\frac{\hbar^2}{2m_{OO}}\frac{\partial^2}{\partial {r_{OO}}^2} - \frac{\hbar^2}{2}\left[\frac{1}{m_{CC}{r_{CC}}^2} + \frac{1}{m_{CO}{r_{CO}}^2}\right]\frac{\partial^2}{\partial {\theta_{CCO}}^2} + \frac{\hbar^2\cos\theta_{CCO}}{m_C r_{CO} r_{CC}}\frac{\partial^2}{\partial\theta_{CCO}\partial r_{CC}}$$

$$+\frac{\hbar^2\cos\theta_{COO}}{m_O r_{CO}}\frac{\partial}{\partial r_{OO}} - \frac{\hbar^2}{2\tan\theta_{CCO}}\left[\frac{1}{m_{CC}{r_{CC}}^2} + \frac{1}{m_{CO}{r_{CO}}^2}\right]\frac{\partial}{\partial\theta_{CCO}}$$

$$-\frac{\hbar^2}{2}\left[\frac{4\sin\theta_{CCO}}{m_C r_{CC} r_{CO}} - \frac{2}{m_C r_{CC} r_{CO}\sin\theta_{CCO}}\right]\frac{\partial}{\partial\theta_{CCO}}$$

$$+V(r_{OO},\theta_{CCO})$$

Lastly, for the methyl rotation in CH_3CHOO, we defined the Hamiltonian using the HCCO dihedral angle φ_{HCCO} and r_{OO},

$$\widehat{H} = -\frac{\hbar^2}{2m_{OO}}\frac{\partial^2}{\partial {r_{OO}}^2} - \frac{\hbar^2}{2I}\frac{\partial^2}{\partial {\varphi_{HCCO}}^2} + V(r_{OO},\varphi_{HCCO})$$

where I is the moment of inertia for the CH_3 group. The 2D wave packet calculation were performed with MCTDH package.[3,4] For r_{OO} we used sine discrete variable representation basis between 1.11 to 2.49 Å with a grid of $\Delta r_{OO} = 2.65\times10^{-2}$, while for θ_{COO}, we used a sine basis between $\theta_{eq} - 45°$ to $\theta_{eq} + 30°$ with a grid of $\Delta\theta_{COO} = 1.15°$. For θ_{CCO}, we used a sine basis between $\theta_{eq} - 30°$ to $\theta_{eq} + 30°$ with a grid of $\Delta\theta_{COO} = 1.15°$. Lastly, for φ_{HCCO}, we used an exponential basis between $\varphi_{HCCO} = 0°$ to $180°$ with a grid of $\Delta\theta_{COO} = 3.5°$.

Below we list the Gaussian width estimated with Schinke's approach[5].

Table S1. The Gaussian width, in eV, calculated using the harmonic ground state, linear excited state approach of Schinke[5]

Molecule	width
CH_2OO	0.28
anti-CH_3CHOO	0.23
syn-CH_3CHOO	0.25

$(CH_3)_2COO$	0.21
anti Anti-$CH_2CHCHOO$	0.28
anti Syn-$CH_2CHCHOO$	0.28
syn Anti-$CH_2CHCHOO$	0.27
syn Syn-$CH_2CHCHOO$	0.27
anti Gau-CH_3CH_2CHOO	0.24
anti Syn-CH_3CH_2CHOO	0.24
syn Anti-CH_3CH_2CHOO	0.26
syn Gau-CH_3CH_2CHOO	0.25
anti-CHCCHOO	0.25
syn-CHCCHOO	0.25

For the calculation of the j-value, we use the following equation.

$$j = \int F(\lambda)\sigma(\lambda)\Phi(\lambda)\ d\lambda$$

where $F(\lambda)$ is the solar actinic flux obtained from the literature[6], and we assumed a quantum yield of unity for the OO dissociation $\Phi(\lambda) = 1$. Using the cross sections $\sigma(\lambda)$ of the UV spectra calculated by the approximations above, we obtain the j-value by numerical integration.

Results and Discussion

Convergence of quantum chemistry methods:

In the Figures S5, we plot the PEC obtained using the equation of motion coupled cluster singles and doubles (EOM-CCSD) method with the aug-cc-pVTZ basis set. Compared to the PEC given by MRCI+Q, the potential well in the 2A' state is narrower and the 2A' potential minima is very close to the GS minimum OO bond length. Furthermore, the crossing between the 2A' and 3A' states also occurs at a shorter OO bond length. The values of the TM are also slightly larger

compared to those obtained from MRCI. As seen from the plots given in Figure S6, this results in a much narrower peak with a much larger cross section for the UV spectra. Furthermore, the peak position is also blue shifted compared to the available experimental results.

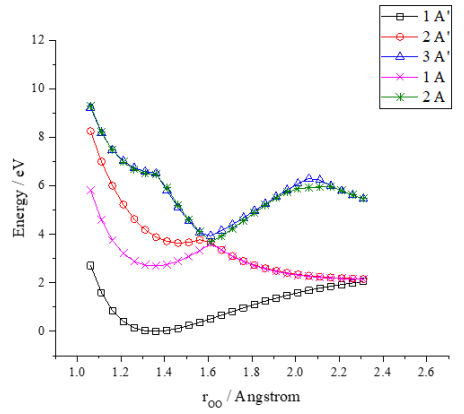

(a) CH_2OO Energy

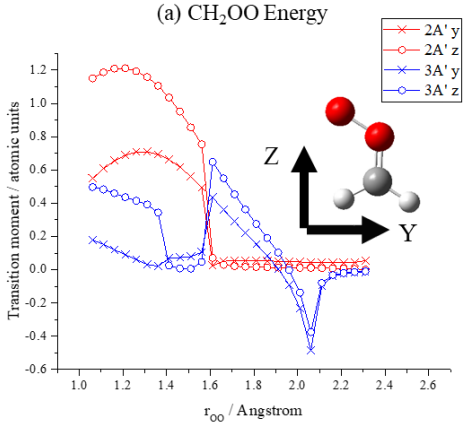

(b) CH_2OO Transition Moment

Figure S5. (a) Potential energy curve for the ground and excited states of CH_2OO calculated using EOM-CCSD/aug-cc-pVTZ. (b) Transition moment curve from the ground state to the 2A' and 3A' states in the Y and Z direction for CH_2OO.

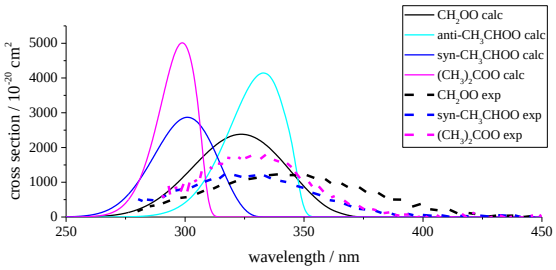

Figure S6. The UV spectra for CH_2OO, CH_3CHOO and $(CH_3)_2COO$ calculated with reflection

approximation, with the EOM-CCSD PEC and the experimental spectra by Lin and coworkers[1,7,8]

In Table S2 we summarize the vertical transition energies calculated at the QCISD(T)/aug-cc-pVTZ equilibrium geometries and previous theoretical values along with the experimental peak position for CH_2OO and CH_3CHOO. First, when we compare with the experimental peak position, the calculated vertical energy using 15 SA-CASSCF (10e 10o) based MRCI+Q(8e 8o)/aug-cc-pVTZ//QCISD(T)/aug-cc-pVTZ overestimate the peak position by 0.2 eV for CH_3CHOO, while giving consistent values for CH_2OO. As can be seen from the comparison of the first three lines the use of (8e, 8o) active space shows converged results with 0.03 eV variation at most for CH_2OO. Next, by comparing the first line with the fourth line, we observe that the basis set effect can be large for CH_2OO where there is a variation of 0.12 eV, but for CH_3CHOO the results by aug-cc-pVTZ seem converged. Although the explicitly correlated MRCI-F12+Q method gives 0.25 eV larger values for (8e, 8o) active space, it becomes ~0.15 eV for the larger (10e 10o) active space. As given in row 8, for CH_3CHOO, the use of a bigger CASSCF active space results in a drastic blue shift in the peak position making it closer to the experimental values compared to the (10e 10o) active space. We note that (14e 15o) active space for CH_3CHOO corresponds to closing all 1s and 2s orbitals for the carbon and oxygen atoms and also closing one extra 2p orbital. For CH_2OO, the aforementioned active space scheme corresponds to (10e 10o) active space. One can notice that the CASSCF, EOM-CCSD, and TD-B3LYP overestimate the vertical transition energies. Compared to the results given by Trabelsi et al. which used EOM-CCSD method at a different geometry, we can see that variation in the equilibrium geometry can also give a 0.1 eV error.

Table S2. The vertical transition energy, in eV, between the ground electronic state and 2A' state for CH_2OO and CH_3CHOO calculated using different quantum chemistry methods. All calculations are performed with the aug-cc-pVTZ basis unless noted otherwise.

	CH_2OO	*anti*-CH_3CHOO	*syn*-CH_3CHOO
MRCI+Q (8e, 8o), SA-CASSCF(10e,10o)	3.68	3.65	4.02
MRCI+Q (10e, 10o), SA-CASSCF(10e,10o)	3.64	3.63	4.03
MRCI+Q (12e, 11o), SA-CASSCF(12e,11o)	3.65		

		3.62	4.02
MRCI+Q (8e, 8o), SA-CASSCF(10e,10o)/aVQZ	3.80	3.67	4.04
MRCI-F12 (8e, 8o), SA-CASSCF(10e,10o)	3.67	3.65	4.03
MRCI-F12+Q (8e, 8o), SA-CASSCF(10e,10o)	3.90	3.88	4.26
MRCI-F12+Q (10e, 10o), SA-CASSCF(10e,10o)	3.63	3.76	4.18
MRCI+Q (10e, 10o), SA-CASSCF(14e,15o)		3.52	3.89
CASSCF(10e,10o)	4.55	4.47	4.64
EOM-CCSD	3.89	3.82	4.19
TD-B3LYP	4.28	4.00	4.39
EOM-CCSD[a]	4.00	3.89	4.28
*MRCI-F12(18e, 14o), SS-*CASSCF(18e,14o)[b]	3.75		
Exp	3.65[c]	3.44[d]	3.78[e]

a: EOM-CCSD results at RCCSD(T)-F12 geometry[9], b: full valance MRCI-F12 results using state specific full valance CASSCF at CCSD(T*)-F12b geometry[10], c: experimental peak position by Ting et al.[1], d: experimental peak position by Sheps et al.[11], e: experimental peak position by Smith et al.[7]

Details of UV spectra calculation:

The results obtained from the WPA for CH_2OO, CH_3CHOO, $(CH_3)_2COO$ and $CH_2CHCHOO$

are given in Figure S7. They all have wide peaks with sharp oscillating features in the long wavelengths. These sharp features are due to the trapping in the 2A' state, and in the present 1D calculation, we overestimate the lifetime of this WP in this potential well. If we consider more degrees of freedom, the decay out of this potential well will be faster and thus wash away many of these sharp features (also see Figure S10). As given in Figure S8, the use of diabatic picture for the first excited state results in a WPA spectrum similar to that of the FCA. More detailed diabatization method was given in the work of Samanta et al.[12], but in the present case, we used a simple diabatization where we exchange the 2A' and 3A' states after the crossing. This diabatization method causes the first excited A' electronic state to be bound. We note that for the RA, the spectra obtained by adiabatic PEC and diabatic PEC are nearly equal to each other and the variation is smaller than the width of the line used to plot it in Figure 2 of the main text.

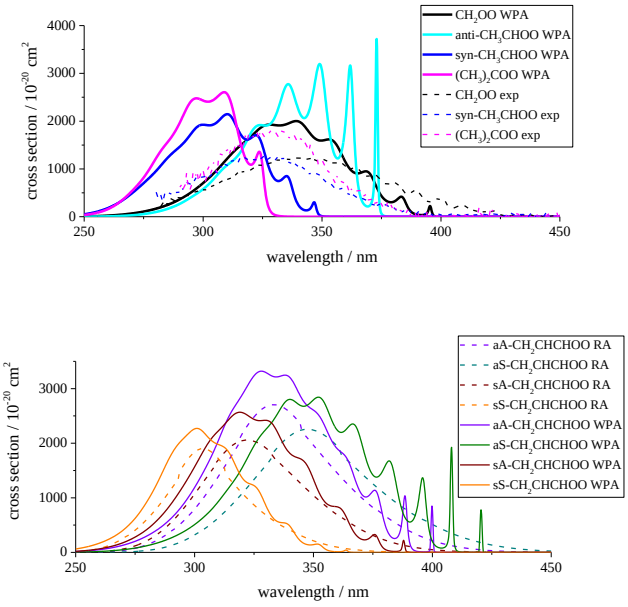

Figure S7. UV spectra of CH_2OO, CH_3CHOO, $(CH_3)_2COO$ and $CH_2CHCHOO$ calculated using the wave packet method on the 2A' adiabatic potential energy curve. The experimental results by Lin and coworkers[1,7,8] are also given.

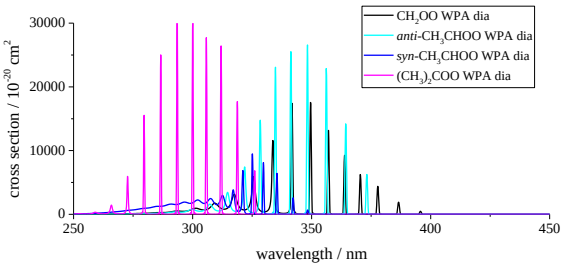

Figure S8. UV spectra of CH_2OO, CH_3CHOO, and $(CH_3)_2COO$ calculated using the wave packet method on the first excited A‘ diabatic potential energy curve.

As given in Figure S9, the transition from the GS to the 1A” state is at least two orders of magnitude weaker than that between GS and 2A’ state. Therefore, we can ignore the contribution for this transition toward the observed spectra in 300-400 nm. It is interesting to note that although very weak, the cross section of this 1A” transition does have a strong substituent dependence.

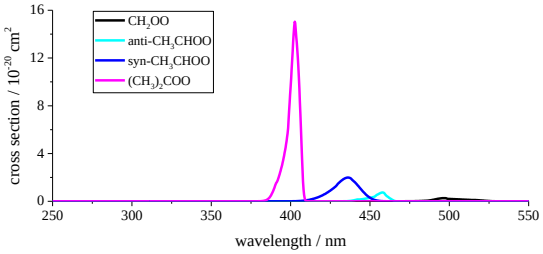

Figure S9. UV spectra of CH_2OO, CH_3CHOO, $(CH_3)_2COO$ and $CH_2CHCHOO$ calculated using the wave packet method on the 1A“ adiabatic potential energy curve.

In Figure S10 we evaluate the change in the UV spectra due to the vibrational coupling of the OO bond to the COO, CCO, and HCCO angles. One can see that the inclusion of other vibrational modes can only give slight modifications to the spectra and that the main contribution comes from the decay along the OO bond. Also, it is clear that the inclusion of the more degrees of freedom will cause the oscillation of sharp peaks seen on the blue side of the 1D results to broaden.

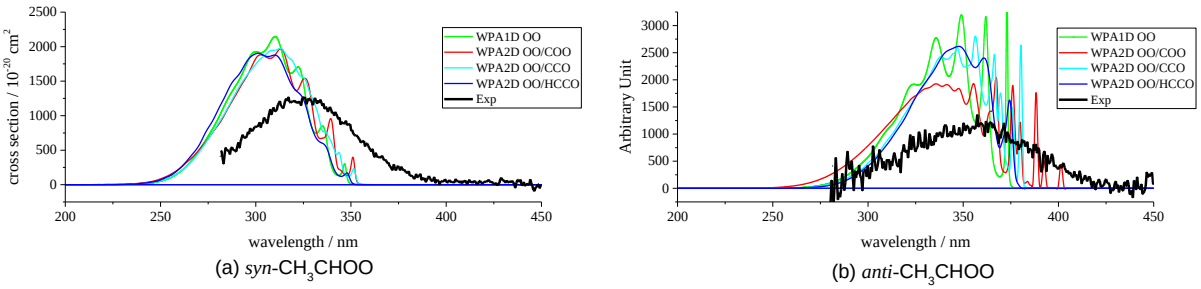

Figure S10. UV spectra of (a) *syn*- and (b) *anti*-CH_3CHOO calculated using the MRCI+Q potential energy surface using 1D wave packet approximation for OO stretching mode (WPD1D), 2D wavepacket approximation for OO stretching and COO bending modes(WP2D OO/COO), 2D wavepacket approximation for OO stretching and CCO bending modes(WP2D OO/CCO), 2D wavepacket approximation for OO stretching and methyl HCCO torsion modes(WP2D OO/HCCO). All the calculation were performed using the PES and TM calcualted by 15 SA-CASSCF (10e 10o) orbitals using MRCI+Q (8e 8o).

Comparison of peak position and peak cross section:

In Table S3, we present the peak position, and the peak cross section obtained using our best quantum chemistry calculation using Schinke's Gaussian model as well as the available experimental values.

Table S3. The peak position, in nm, and peak cross section in 10^{-17} cm^2

Molecule	Peak position	Peak cross section
CH_2OO	342 (340)[a]	1.39 (1.2)[a]
anti-CH_3CHOO	352 (360)[b]	1.61 (1.2)[b]
syn-CH_3CHOO	319 (328)[c]	1.29 (1.27)[c]
$(CH_3)_2COO$	306 (330)[d]	2.16 (1.75)[d]
anti Gau-CH_3CH_2CHOO	335	1.94
anti Syn-CH_3CH_2CHOO	331	1.87

syn Anti-CH_3CH_2CHOO	303	1.59
syn Gau-CH_3CH_2CHOO	310	1.52
anti Anti-$CH_2CHCHOO$	378	4.64
anti Syn-$CH_2CHCHOO$	407	3.69
syn Anti-$CH_2CHCHOO$	395	3.91
syn Syn-$CH_2CHCHOO$	361	2.69
anti-CHCCHOO	351	2.31
syn-CHCCHOO	351	1.54

a: experimental results by Ting et al.[1] b: experimental results by Sheps et al.[11] c: experimental results by Smith et al.[7] d: experimental results by Chang et al.[8]

J-value at different solar zenith angles:

The j-values at different solar zenith angles are given in Table S4. The general conclusion is similar to that of 0°, where the substituent dependence is small.

Table S4. The j-values at different solar zenith angles for the Criegee intermediates calculated using the Gaussian convolution of the equilibrium peak position and oscillator strength.

Molecule	30°	60°
CH_2OO	0.14 (0.15)[a]	0.09 (0.09)[a]
anti-CH_3CHOO	0.16 (0.19)[a]	0.09 (0.12)[b]
syn-CH_3CHOO	0.05 (0.07)[a]	0.02 (0.04)[b]
$(CH_3)_2COO$	0.03	0.01
anti Anti-$CH_2CHCHOO$	0.25 (0.77)[a]	0.15 (0.52)[c]
anti Syn-$CH_2CHCHOO$	0.29 (1.00)[a]	0.19 (0.71)[c]
syn Anti-$CH_2CHCHOO$	0.14 (0.69)[a]	0.08 (0.48)[c]
syn Syn-$CH_2CHCHOO$	0.05 (0.29)[a]	0.03 (0.19)[c]

anti Gau-CH_3CH_2CHOO	0.15	0.09
anti Syn-CH_3CH_2CHOO	0.13	0.07
syn Anti-CH_3CH_2CHOO	0.04	0.02
syn Gau-CH_3CH_2CHOO	0.05	0.03
anti-CHCCHOO	0.66 (0.32)[a]	0.44 (0.21)[d]
syn-CHCCHOO	0.41 (0.20)[a]	0.27 (0.13)[d]

a: (18e 14o) active space, b: (14e 15o) active space c: (14e 15o) active space d: (14e 14o) active space

Direction of transition moment:

For the photolysis of CH_2OO, Lester and coworkers experimentally determined the angle between the transition moment of the UV transition and the OO bond. They obtained a constant value of 37° for the range between 300 to 400 nm.[13] This observation gave proof that the spectra are coming from excitation to one electronic state. As given in Table S5, the angles between the transition moment between the ground electronic state and the 2A' state calculated by MRCI+Q (8e 8o) from CASSCF (10e 10o) and EOM-CCSD give values that are consistent to those obtained by Lester and coworkers. This similarity gives further justification that the spectra observed experimentally are the transition to the 2A' state. As shown above, the only other transition in this wavelength range is from the ground electronic state to the 1A" state, but this transition will be much weaker in cross section, see Figure S8.

Table S5. The tilt angle of the transition moment between the electronic ground state and the first excited A' state with respect to the OO bond. The results are from the MRCI (8e, 8o) and CCSD-EOM methods with the aug-cc-pVTZ basis.

Molecule	MRCI (8e 8o)	CCSD-EOM
CH_2OO	28.6 (37[a])	30.3
anti-CH_3CHOO	27.0	27.4
syn-CH_3CHOO	34.4	40.1

$(CH_3)_2COO$	32.4	36.2
anti Anti-$CH_2CHCHOO$	18.6	12.2
anti Syn-$CH_2CHCHOO$	28.2	30.1
syn Anti-$CH_2CHCHOO$	38.7	50.2
syn Syn-$CH_2CHCHOO$	43.3	66.2
anti Gau-CH_3CH_2CHOO	27.1	27.7
anti Syn-CH_3CH_2CHOO	25.9	25.2
syn Anti-CH_3CH_2CHOO	33.7	41.5
syn Gau-CH_3CH_2CHOO	34.4	41.4
anti-CHCCHOO	56.2	55.1
syn-CHCCHOO	24.6	22.8

References

1 W.-L. Ting, Y.-H. Chen, W. Chao, M. C. Smith and J. J.-M. Lin, *Phys. Chem. Chem. Phys.*, 2014, **16**, 10438–10443.

2 N. C. Handy, *Mol. Phys.*, 1987, **61**, 207–223.

3 M. H. Beck, A. Jackle, G. A. Worth and H.-D. Meyer, *Phys. Rep.*, 2000, **324**, 1–105.

4 H.-D. Meyer and G. a. Worth, *Theor. Chem. Acc.*, 2003, **109**, 251–267.

5 R. Schinke, *Photodissociation Dynamics: Spectroscopy and Fragmentation of Small*

Polyatomic Molecuels, Cambridge Univeristy Press, Cambridge, 1993.

6 B. J. Finlayson-Pitts and J. N. Pitts Jr, *Chemistry of the upper and lower atmosphere: theory, experiments, and applications*, Academic Press, San Diego, 2000.

7 M. C. Smith, W.-L. Ting, C. Chun-Hung, K. Takahashi, K. A. Boering and J. J.-M. Lin, *J. Chem. Phys.*, 2014, **141**, 74302.

8 Y. P. Chang, C. H. Chang, K. Takahashi and J. J. M. Lin, *Chem. Phys. Lett.*, 2016, **653**, 155–160.

9 T. Trabelsi, M. Kumar and J. S. Francisco, *J. Chem. Phys.*, 2017, **147**, 164303.

10 R. Dawes, B. Jiang and H. Guo, *J. Am. Chem. Soc.*, 2014, **137**, 50–53.

11 L. Sheps, A. M. Scully and K. Au, *Phys. Chem. Chem. Phys.*, 2014, **16**, 26701–26706.

12 K. Samanta, J. M. Beames, M. I. Lester and J. E. Subotnik, *J. Chem. Phys.*, 2014, **141**, 134303.

13 M. F. Vansco, H. Li and M. I. Lester, *J. Chem. Phys.*, 2017, **147**, 13907.

XYZ geometries calculated by QCISD(T)/aug-cc-pVTZ

CH_2OO

C	0.00000000	0.00000000	0.00000000
O	0.00000000	0.00000000	1.25430000
O	1.17982006	0.00000000	1.91290919
H	0.94413785	0.00000000	-0.53015051
H	-0.97698441	-0.00000000	-0.46079660

anti-CH_3CHOO

C	0.00000000	0.00000000	0.00000000
O	0.00000000	0.00000000	1.25520000

H	0.97004354	0.00000000	-0.48849641
C	-1.29014151	-0.00000000	-0.72132829
H	-1.35790291	0.87742454	-1.36971257
H	-1.35790291	-0.87742454	-1.36971257
H	-2.12445269	-0.00000000	-0.02455441
O	1.20184541	0.00000000	1.91344744

syn-CH_3CHOO

C	0.00000000	0.00000000	0.00000000
O	0.00000000	0.00000000	1.26180000
H	0.99787635	0.00000000	-0.42112752
C	-1.24378669	-0.00000000	-0.77749399
H	-1.04460429	-0.00000000	-1.84507179
H	-1.84611040	-0.86701589	-0.48980799
H	-1.84611040	0.86701589	-0.48980799
O	-1.21507591	-0.00000000	1.88964857

$(CH_3)_2COO$

C	0.00000000	0.00000000	0.00000000
O	0.00000000	0.00000000	1.26560000
O	1.22394436	0.00000000	1.90392935
C	-1.33708080	-0.00000000	-0.64976496
H	-1.44315356	0.87768836	-1.29178246
H	-1.44315356	-0.87768836	-1.29178246
H	-2.12846249	-0.00000000	0.09511708
C	1.28086658	0.00000000	-0.72901800
H	1.86940853	0.86524605	-0.41235961
H	1.86940853	-0.86524605	-0.41235961
H	1.13041370	0.00000000	-1.80505061

anti_Syn-CH_3CH_2CHOO

C	0.00000000	0.00000000	0.00000000
O	0.00000000	0.00000000	1.25346924
O	1.20665231	0.00000000	1.91270553
H	0.97071145	0.00000000	-0.48848009
C	-1.28351764	-0.00000000	-0.74377792

H	-1.26778134	0.86720835	-1.41472510
H	-1.26778134	-0.86720835	-1.41472510
C	-2.54302020	-0.00000000	0.11952213
H	-3.42717506	-0.00000000	-0.51546195
H	-2.58222922	-0.87907964	0.76049410
H	-2.58222922	0.87907964	0.76049410

anti_Gauche-CH_3CH_2CHOO

C	0.00000000	0.00000000	0.00000000
O	0.00000000	0.00000000	1.25526013
O	1.20214961	0.00000000	1.91478973
H	0.97109218	0.00741170	-0.48840576
C	-1.28997858	0.00690664	-0.72992609
H	-2.10350289	-0.04686618	-0.00784420
H	-1.33420018	-0.89858008	-1.34421973
C	-1.43683860	1.23952372	-1.64101336
H	-0.62043347	1.30157543	-2.36053879
H	-2.37066090	1.17947606	-2.19792938
H	-1.44564641	2.15841058	-1.05674554

syn_Anti-CH_3CH_2CHOO

C	0.00000000	0.00000000	0.00000000
O	0.00000000	0.00000000	1.26145764
O	1.21681473	0.00000000	1.88979664
H	-0.99916478	-0.00000000	-0.42188947
C	1.23950382	0.00000000	-0.79073821
H	1.83314380	0.85797134	-0.45236754
H	1.83314380	-0.85797134	-0.45236754
C	1.01204507	-0.00000000	-2.30095442
H	1.96512007	-0.00000000	-2.82662348
H	0.45808956	0.88236250	-2.62261693
H	0.45808956	-0.88236250	-2.62261693

syn_Gauche-CH_3CH_2CHOO

C	0.00000000	0.00000000	0.00000000
O	0.00000000	0.00000000	1.26213713

O	1.20596387	0.00000000	1.91046588
H	-1.00321731	-0.00542233	-0.41086451
C	1.23196430	0.00308925	-0.80991773
H	0.98719473	0.33688350	-1.81781137
H	1.91966032	0.71284401	-0.34429315
C	1.90895291	-1.38693094	-0.85055058
H	1.26332266	-2.12663143	-1.32253942
H	2.82935511	-1.32108347	-1.42854488
H	2.15204957	-1.71534706	0.15630250

anti_Anti-$CH_2CHCHOO$

C	0.00000000	0.00000000	0.00000000
O	0.00000000	0.00000000	1.26844732
O	1.20075318	0.00000000	1.90791465
H	0.96637104	0.00000000	-0.49327807
C	-1.24893812	-0.00000000	-0.69092637
H	-2.14310459	-0.00000000	-0.08119145
C	-1.31663675	-0.00000000	-2.03022010
H	-2.26612698	-0.00000000	-2.54408852
H	-0.42420620	0.00000000	-2.64166256

anti_Syn-$CH_2CHCHOO$

C	0.00000000	0.00000000	0.00000000
O	0.00000000	0.00000000	1.26694779
O	1.19938637	0.00000000	1.91213598
H	0.97108640	0.00000000	-0.48254555
C	-1.23693438	-0.00000000	-0.73338706
H	-1.12042454	-0.00000000	-1.80920521
C	-2.46299945	-0.00000000	-0.19130760
H	-3.34221132	-0.00000000	-0.81809000
H	-2.61228870	-0.00000000	0.87901543

syn_Anti-$CH_2CHCHOO$

C	0.00000000	0.00000000	0.00000000
O	0.00000000	0.00000000	1.27266608
O	1.18674278	0.00000000	1.93957809

H	-1.00016406	-0.00000000	-0.41568905
C	1.17500724	0.00000000	-0.81135196
H	2.11874805	0.00000000	-0.28665950
C	1.09073457	-0.00000000	-2.14936191
H	0.13605235	-0.00000000	-2.65998530
H	1.97641558	-0.00000000	-2.76769352

syn_Syn-$CH_2CHCHOO$

C	0.00000000	0.00000000	0.00000000
O	0.00000000	0.00000000	1.27624578
O	1.18232274	0.00000000	1.94676619
H	-1.01188004	-0.00000000	-0.38564176
C	1.11204052	0.00000000	-0.88945447
H	0.82819616	-0.00000000	-1.93479769
C	2.41919550	0.00000000	-0.55849309
H	2.73066599	0.00000000	0.47115785
H	3.16374956	-0.00000000	-1.34368137

anti-CHCCHOO

C	0.00000000	0.00000000	0.00000000
O	0.00000000	0.00000000	1.27289664
O	1.19201932	0.00000000	1.90250162
H	0.96219126	0.00000000	-0.49883495
C	-1.22138238	-0.00000000	-0.68309343
C	-2.23111418	-0.00000000	-1.33826867
H	-3.13189334	-0.00000000	-1.90135085

syn-CHCCHOO

C	0.00000000	0.00000000	0.00000000
O	0.00000000	0.00000000	1.27638146
O	1.17536815	0.00000000	1.92965487
H	-0.99211687	-0.00000000	-0.42911652
C	1.15973266	0.00000000	-0.77885744
C	2.11344063	-0.00000000	-1.51290815
H	2.97108724	-0.00000000	-2.13975561